Properties of polyamide 6 and polyvinylidene fluoride nanofibers irradiated by H^+ ions

Eva Štěpanovská[1,2*], *Petr* Malinský[1,2], *Jindřich* Matoušek[2], *David* Poustka[2], *Anna* Macková[1,2]

[1]Nuclear Physics Institute of the Czech Academy of Science, *v. v. i., 250 68 Rez, Czech Republic*

[2]Department of Physics, Faculty of Science, J.E. Purkyne University, Pasteurova 3632/15, 400 96 Ústí nad Labem, Czech Republic

Abstract. This work deals with the modification of polymeric nanofibers of polyamide 6 (PA6) and polyvinylidene fluoride (PVDF) which were formed by electrospinning process. After the manufacturing process, the polymer nanofibers were exposed to the implantation of 1 MeV H^+ ions on a tandem accelerator Tandetron MC 4130. The ion implantation was provided with different ion fluences (1.8; 3.7; 5.6)×10^{14} cm^{-2}. Ion implantation of polymer nanofibers can modify their functional properties due to ion interaction with nanofibers changing their structure and elemental composition. H-ion interaction with nanofibers was simulated by SRIM program which shows the modification of polymers by prevailing electronic stopping. Rutherford Back-Scattering spectrometry (RBS) and Elastic Recoil Detection Analysis (ERDA) show distinct elemental modification in the irradiated layer of PVDF and PA6 nanofibers. The changes in surface chemistry was identified by X-ray Photoelectron Spectroscopy (XPS). The identified chemical changes contributed to the changes of electrical properties (increase of electrical conductivity) being measured by the standard two-point method.

1 Introduction

Polymer nanofibers are a widely studied material. Due to their large effective area and porous structure, electrospun nanofibers can be employed in a wide range of applications [1,2]. When the modification of nanofibers leads to increase of their electrical conductivity and morphological changes, they can be used in fields such as electronics [3] or sensorics [4]. Although nanofibers have a diameter in the range of 1-100 nm, they mostly retain mechanical properties of bulk polymer. However, most modifications (e.g plasma, UV-light etc.) affect only chemical bonds on the surface. In this work, the modification of nylon 6 (PA6) and polyvinylidene fluoride (PVDF) nanofibers by the ion beam irradiation is followed. Ion beam interaction with nanofibers can change their electronic structure, chemical composition and it can lead to a change in polymer crystallinity, nanofiber morphology and electrical properties [5]. We have chosen irradiation by 1 MeV H^+ ions into polymer nanofibers, where

* Corresponding author: stepanovska@ujf.cas.cz

© The Authors, published by EDP Sciences. This is an open access article distributed under the terms of the Creative Commons Attribution License 4.0 (http://creativecommons.org/licenses/by/4.0/).

mainly electronic stopping is employed in the modified layer withouth significant disruptive ballistic processes and experiencing high penetration depth.

2 Experimental

For our purposes, electrostatic spinning was performed on the NS 1WS500U device (Elmarco, CZ). PVDF fibres were formed from 12 wt. PVDF solution. This solution was performed by mixing of 12 g of PVDF powder (Solvay, Belgium), 86.8 g of N, N-dimethylformamide (Penta, CZ) and 1.2 g of tetrabuthylammonium bromide (Sigma Aldrich, UK). The mixture was heated and stirred at 70 °C for 5 hours. The procedure for the formation of PA6 solution is given e.g. in [6]. The electrostatic spinning parameters are given in Tab.1.

Table. 1. Parameters of electrospinning on the NS 1WS500U device.

Parameters of electrospinning	**PVDF**	**PA6**
Distance of electrodes (mm)	180	240
Cathode voltage (V)	10	30
Anode voltage (V)	50	60
Winding of spoundbound (mm/min)	45	30
Humidity (%)	27	38
Temperature (K)	294.85	297.65

The prepared nanotextiles of PA6 and PVDF were further modified by implantation of H^+ ions with 1 MeV energy at the implantation fluences (1,8: 3,7: 5,6) × 10^{14} cm^{-2}. The ion beam was steered over area of 5×5 cm, directed vertically on the sample surface. The ion current during the irradiation was kept ~15-45 $nA.cm^{-2}$.

The PA6 and PVDF elemental composition was studied on the 1 MeV H^+ ions-irradiated samples using RBS and ERDA. The RBS/ERDA spectra were collected using 1.7 MeV He^+ ion beams. An Ultra-Ortec PIPS detector recorded backscattered He ions in Cornell geometry with a laboratory scattering angle of 170°. The ERDA primary beam incoming angle was 75° and the scattering angle was 30°. The recoiled particles were recorded by Canberra PIPS detector covered by 12 μm Mylar foil. The ion currents used during the RBS and ERDA analyses were ~5 nA. Several RBS spectra were collected at different sample parts to reduce the effects of sample degradation, with the final spectrum obtained by summing the individual spectra. The elemental concentration was analysed using the SIMNRA code [7].

The ion projected ranges and energy losses of the H^+ 1 MeV ion beam in the PA6 and PVDF nanofibers were calculated by the SRIM full-cascade Monte-Carlo simulation [8], version Stopping power SRIM-2008 . The elemental composition of the PA6 and PVDF pristine sample used for the SRIM simulation was determined by RBS and ERDA (PA6: C – 58 %, H – 22%, O – 9 %, N – 11 % and PVDF: C – 62 %, H – 12 %, O – 3 %, F – 24 %). The density of PA6 (1.084 g/cm^3) was used from publication [9] and the density of PVDF (1.78 g/cm^3) was used from publication [10].

3 Results and discussion

3.1 SRIM

The SRIM-calculated electronic (S_e) and nuclear (S_n) stopping in the near-surface layer, the energy stopping ratio (S_e/S_n) and the projected range (R_P) of H^+ ions are presented in Table 2. Furthermore, the integral of electronic ($S_e(\int)$) and nuclear ($S_n(\int)$) stopping was determined in order to find the total electronic and nuclear energy loss of H-ions on the whole penetration range.

Table. 2. Data obtained from SRIM: R_P is the projected range of H^+ 1MeV ions, ΔR_P is the standard deviation of the ion depth distribution , S_e is the value of electronic stopping at the surface for a given polymer and S_n is the value of nuclear stopping, S_e/S_n is the ratio between electronic and nuclear stopping at the surface, $S_e(\int)$ is integral value of electronic stopping in the whole penetrated volume, $S_n(\int)$ is the value of nuclear stopping in the whole penetrated volume and $S_e(\int)/S_n(\int)$ is the ratio between electronic and nuclear integral stopping.

Nanofibers/ Ions	R_P (μm)	ΔR_P (μm)	S_e (eV/nm)	S_n (eV/nm)	S_e/S_n (eV/nm)	$S_e(\int)$ (eV/nm)	$S_n(\int)$ (eV/nm)	$S_e(\int)/S_n(\int)$ (eV/nm)
PA6/H^+	26.8	6.7	24.26	0.01	2426	$99{,}4\times10^4$	1044.7	952
PVDF/H^+	17.1	4.2	38.44	0.01	3844	$99{,}2\times10^4$	1071.7	926

The depth profiles of S_e and S_n ion energy losses together with 1 MeV H^+ depth distribution in PA6 and PVDF are depicted in Fig. 1a and 1b, respectively. The 1 MeV H^+ ions mostly lose their energy through the electronic stopping processes in both nanofiber layers (see Table 2 and Fig. 1) and the ratios of the electronic (S_e) and nuclear (S_n) stopping power of 1 MeV H^+ ions in PA6 and PVDF show the prevailing electronic stopping as well. During this process, electrons are released and chemical bonds are broken, the ejections of matrix atoms is rather unlike due to the low mass of H^+ ions undergoing negligible nuclear stopping. H-ion projected ranges don't cover the whole thickness of the nanofiber layers being in total about 66 μm for PA6 and about 60 μm for PVDF.

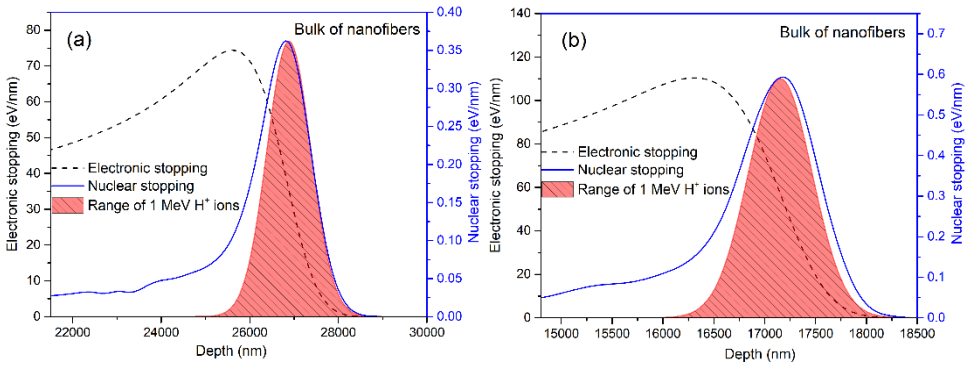

Fig. 1. The SRIM calculation of the electronic and nuclear energy stopping of 1 MeV H^+ ions vs. depth and the 1 MeV H^+ ion depth profiles in PA6 (a) and PVDF (b).

3.2 RBS and ERDA analysis of elemental compositions

The elemental composition of PA6 and PVDF nanofibers before and after the H-ion irradiation was determined using RBS and ERDA analytical methods. The accessible information depth of RBS using 1.7 MeV He-ions in both polymers is about 1 μm. The ERDA provides information up to the maximum depth of about 0.5 μm. RBS and ERDA spectra for the pristine and irradiated samples with the H-ion fluence of 3.75×10^{14} cm^{-2} are shown in Fig. 2(a), (b) for PA6 and (c), (d) for PVDF, respectively. The compositional changes are observed in PA6 after the H-ion irradiation (see Fig. 2(a) and (b)) mainly for C and H content. The composition of the irradiated nanofiber layers for all H-ion implantation fluences are summarized in Table 3. The C/O and C/N ratio slightly increases with increasing ion fluence in PA6, carbon content enhancement occurs already for the lowest ion implantation fluence and then for the higher irradiation fluences the carbon concentration stays constant. Hydrogen content is significantly decreased with the increasing H-ion fluence in the whole investigated surface nanofiber layer about 0.5 μm. PVDF (see Fig. 2(c) and (d)) exhibits a more significant change in elemental composition after the H-ion irradiation.

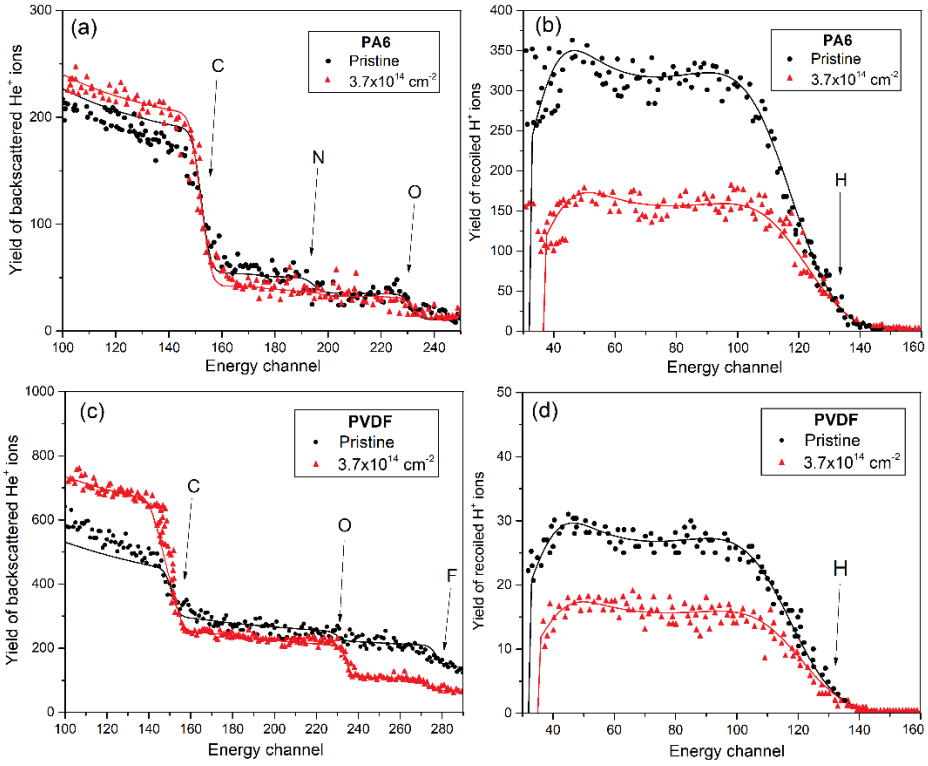

Fig. 2. RBS experimental (points) and SIMNRA simulated (line) spectra for PA6 (a) and PVDF (c) are presented together with ERDA experimental (SIMNRA simulated (line) spectra for PA6 (b) and PVDF (d)).

It should be noted that the oxygen found in the PVDF nanofibers is present due to the blending of the PVDF polymer with DMF (see chapter 2), because oxygen is not present in the PVDF stoichiometry. In PVDF, C/F ratio increases, and significant carbon concentration enhancement occurs with the increased H-ion implantation fluence simultaneously with H, F depletion (see Table 4). For avoiding unintentional effect of the He-ion irradiation during the RBS and ERDA analysis the typical He-ion current about ~ 5 nA was used and to reduce

effects of the sample degradation, several spectra were measured on different beam spots and the final spectrum was obtained by summing the individual spectra.

Table 3. The PA6 stoichiometry before and after the H-ion irradiation determined using RBS and ERDA methods.

	Atomic concentration (%)						
Substrate	C	O	H	N	Impurities (Na, P, K, Mg)	C/O	C/N
PA6 Pristine	58 ± 5	9 ± 2	22 ± 4	11 ± 1	0.1	6	6
PA6/H^+ 1.8x10^{14} cm^{-2}	69 ± 6	8 ± 2	15 ± 3	8 ± 1	0.6	9	9
PA6/H^+ 3.7x10^{14} cm^{-2}	69 ± 6	8 ± 2	14 ± 3	7 ± 1	2	9	10
PA6/H^+ 5.6x10^{14} cm^{-2}	69 ± 6	7 ± 2	15 ± 3	6 ± 1	3	10	12

Table 4. The PVDF stoichiometry before and after the H-ion irradiation determined using RBS and ERDA methods.

Atomic concentration (%)						
Substrate	C	O	H	F	Impurities (Na, P, K, Mg)	C/F
PVDF Pristine	62 ± 5	3	12 ± 2	24 ± 3	0.1	3
PVDF/H^+ 1.8x10^{14} cm^{-2}	87 ± 8	1	5 ± 1	7 ± 1	0.9	12
PVDF/H^+ 3.7x10^{14} cm^{-2}	86 ± 8	1	4 ± 1	8 ± 1	1.0	10
PVDF/H^+ 5.6x10^{14} cm^{-2}	88 ± 8	1	4 ± 1	7 ± 1	0.6	13

3.3 X-ray photoelectron spectroscopy

X-ray photoelectron spectroscopy (XPS), providing information from only a few-nanometre-thick surface layer, was used to examine surface chemistry modification and to identify functional groups on PA6 and PVDF surfaces before and after H-ion irradiation. Fig. 3 shows the C 1s peak and its deconvolution with identification of individual contribution of chemical bonds, where Fig. 3(a) shows the spectrum of C 1s peak of unmodified PA6 nanofibers, Fig. 3(b) PA6 nanofibers irradiated with H-ions, ion implantation fluence of 1.8×10^{14} cm^{-2} and Fig. 3(c) PA6 nanofibers irradiated with H-ions with ion implantation fluence of 5.6×10^{14} cm^{-2}. The C 1s peak of pristine PA6 nanofibers has three different carbon bonding states (Fig. 3): C-C (284.5 eV), C-N, C-O (286.3 eV) and C=O (287.7 eV). These chemical bonds remained present in all PA6 nanofibers after the H-ion implantation. The binding energy values with the percentage of appropriate chemical bonds are presented in Tab. 5. The percentage of C-C bonds was reduced at the lowest ion fluence, while C-N and C-O bonds were increased. With increasing ion fluence, an increase in C-C bonds and a decrease in C-O and C-N bonds were observed. The C=O bonds remains practically constant.

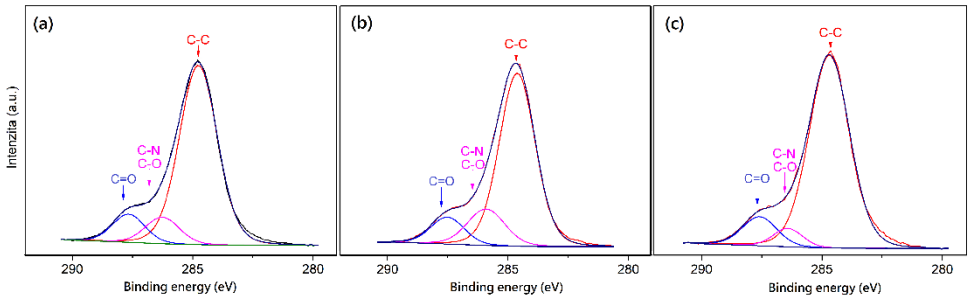

Fig. 3. The deconvolution of the C 1s peak from XPS spectra of (a) pristine PA6, (b) modified PA6 nanofibers with the ion implantation fluence 1.8×10^{14} cm^{-2} and (c) modified PA6 nanofibers with the with ion implantation fluence 5.6×10^{14} cm^{-2}.

Fig. 4 shows the C 1s peak and its deconvolution with identification of individual contribution of chemical bonds in PVDF, where Fig. 4(a) shows the spectrum of C 1s peak of the unmodified PVDF nanofibers, Fig. 4(b) the modified PVDF nanofibers with H^+ ion implantation fluence of 1.8×10^{14} cm^{-2} and Fig. 4(c) the modified nanofibers PVDF by H^+ ion implantation fluence of 5.6×10^{14} cm^{-2}. The C 1s peak of pristine PVDF nanofibers has four different carbon bonding states (Fig. 4a): CH_2, C-C (284.5 eV), C-F (289.6 eV), CF_2 (291.7 eV) and CF_3 (294.6 eV). These chemical bonds remained present in all PVDF nanofibers after H-ion implantation.

Table 5. Position and abundance of the individual components of the C 1s peak in pristine and H-ion irradiated PA6 nanofibers.

PA6/H^+			
Sample	**C-C**	**C-N, C-O**	**C=O**
	Binding energy (eV) / Percentage (%)		
Pristine	284.8/79.0	286.3/10.5	287.7/10.5
1.8×10^{14} cm^{-2} (H^+)	284.8/73.3	286.1/16.1	287.7/10.6
5.6×10^{14} cm^{-2} (H^+)	284.8/83.5	286.5/5.8	287.7/10.7

The binding energy values with the percentage of particular bonds in PVDF are presented in Tab. 6. Fig. 4a and 4b shows a decrease in the signal intensity of all fluorine-containing bonds after implantation of H-ions. In Tab. 6, an increase in C-C, CH_2 bonds was noted, while all fluorine-containing bonds decreased with the increasing H-ion implantation fluence. During irradiation, the enhancement of C-C bonds occurs on the surface of the polymer nanotextile at the expense of defluorination. The increasing carbonization with decrease of fluorine was also confirmed by the RBS analysis, where the trend with increased H-ion irradiation fluence is the same.

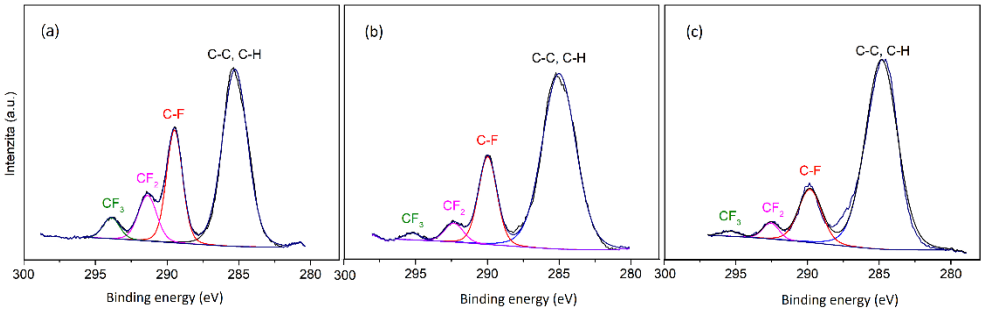

Fig. 4. The deconvolution of the C 1s peak from XPS spectra of pristine PVDF (a), modified PVDF nanofibers with H-ion implantation fluence 1.8×10^{14} cm^{-2} (b) and (c) modified PA6 nanofibers with H-ion implantation fluence 5.6×10^{14} cm^{-2}.

Table 6. Position and abundance of the individual components of the C 1s peak in pristine and H-ion irradiated PVDF nanofibers .

PVDF/H^+				
Sample	**C-C, CH_2**	**C-F**	**CF_2**	**CF_3**
	Binding energy (eV) / Percentage (%)			
Pristine	284.8/59.9	289.6/24.2	291.7/11.3	294.6/4.6
1.8×10^{14} cm^{-2} (H^+)	284.8/79.4	289.7/16.1	292.5/3.3	295.5/1.2
5.6×10^{14} cm^{-2} (H^+)	284.8/73.8	289.8/20.5	292.1/4.4	295.0/1.3

3.4 Electrical properties

Changes in the elemental composition and chemical bonds affected the electrical properties of the modified nanofibers. Fig. 5 shows the IV-characteristics and sheet resistance of PA6 (a, b) and PVDF (c, d) nanofibers irradiated with the different H-ion fluences. As illustrated in Fig. 5(a) and 5(b), with the exception of the H-ion irradiated PA6 nanofibers with a ion fluence of $3.7x10^{14}$ cm^{-2}, it can be said that the sheet resistance is a decreasing after H-ion irradiation and it can be concluded that the predominant electronic stopping of H-ions (see Fig. 1(a)) leads to the increase of C-C bonds and it improves the conductivity of the polymer nanotextile [11]. The values of measured sheet resistances are comparable to the values in literature e.g. [12]. Fig. 5(d) shows a plot of the sheet resistance measured on irradiated PVDF nanofibers. It is evident that the sheet restistance decreases after the H-ion irradiation at the lowest ion fluence. The sheet resistance increases again with the further increase of ion fluence, but it is still lower than the value of pristine PVDF nanofibers. The slight increase in sheet resistance, with increasing ion fluence, may be due to the deteriorated morphology of the nanofibers. It can be assumed that the H-ion irradiation enhances the conductivity of PVDF, but also disrupts the morphology of the nanofibers.

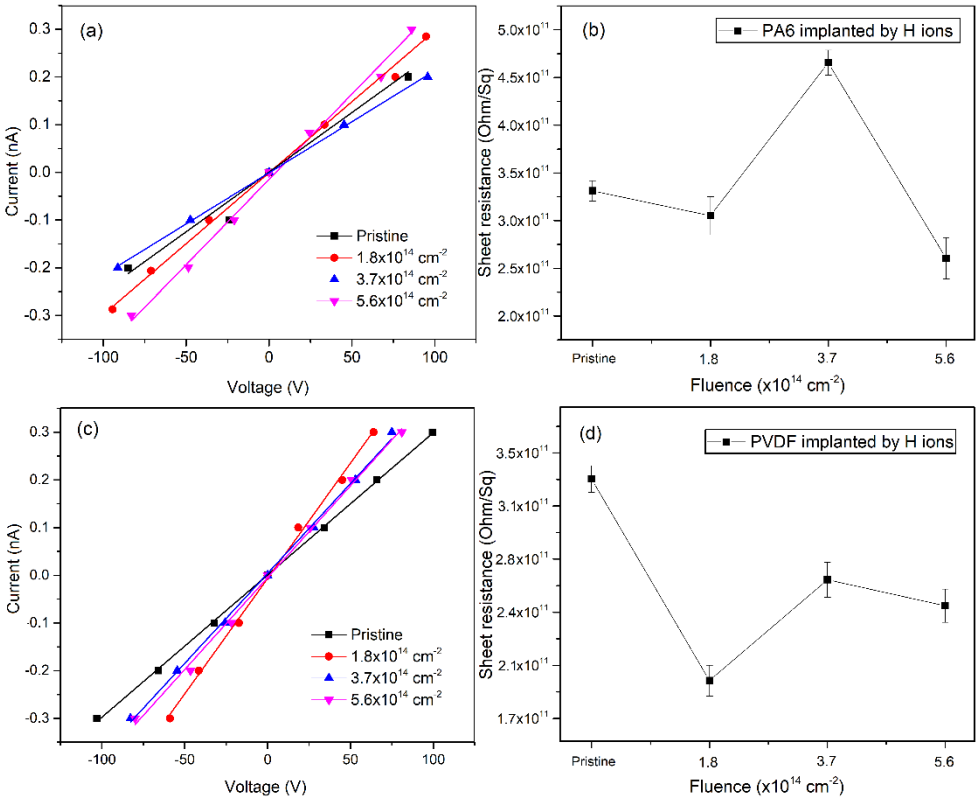

Fig. 5. IV-characteristics of modified PA6 (a) and PVDF nanofibers (c) with sheet resistance of the H-ion irradiated PA6 (b) and PVDF (d) using the various H-ion irradiation fluences.

4 Conclusions

In this work, the polymer nanofibers PA6 and PVDF irradiated by H^+ ions with different fluences (1.8; 3.7; 5.6)×10^{14} cm^{-2} were studied. Using spectrometric and spectroscopic techniques (RBS, ERDA, XPS), changes in the elemental and chemical composition were observed which were caused mainly by electronic stopping of H-ions, as demonstrated by the SRIM calculations. Due to the predominant electronic stopping, the carbon content enhancement occurred in the PA6 polymer, accompanied by N and H depletion. The decrease of C-N bonds on the surface and the increase of C-C bonds was confirmed by XPS.

In the case of PVDF, there were more significant chemical and elemental changes than in PA6. RBS confirmed increase of carbon content with strong defluorination dependent on the increasing ion implantation fluence. The assumption of carbonization and defluorination was also confirmed by the XPS method.

In both PA6 and PVDF, there was a slight increase in electrical conductivity. In both cases, the conductivity was higher for the lower ion fluence and with increasing ion fluence, the conductivity decreased again. This conductivity reduction was probably caused by the morphological degradation of polymeric nanofibers. In general, PVDF exhibited more significant correlation of electrical conductivity increase with the increased H-ion fluence compared to PA6. This fact could be connected to more significant elemental modification and chemical bond disruption in PVDF compared to PA6, as it was shown by RBS and XPS.

Acknowledgement

The research has been carried out at the CANAM (Centre of Accelerators and Nuclear Analytical Methods) infrastructure LM 2015056. This publication was supported by OP RDE, MEYS, Czech Republic under the project CANAM OP, CZ.02.1.01/0.0/0.0/16_013/0001812 and by the Czech Science Foundation (GACR No. 19-02482S) and by the University of J.E.Purkyne project UJEP-SGS-2021-53-005-2.

References

1. S. Ramakrishna, *An Introduction to Electrospinning and Nanofibers*, Hackensack, Nj: World Scientific, 2005
2. A. L. Yarin, B. Pourdeyhimi, S. Ramakrishna, *Fundamentals and Applications of Micro- and Nanofibers*, 2014
3. L. Persano, A. Camposeo, D. Pisignano, *Active polymer nanofibers for photonics, electronics, energy generation and micromechanics*, Progress in Polymer Science, 2015, 43, 48-95
4. Y. Gao, F. Guo, P. Cao, et al. *Winding-Locked Carbon Nanotubes/Polymer nanofibers Helical Yarn for Ultrastretchable Conductor and Strain Sensor*, ACS Nano, 2020, 14(3), 3442-3450
5. M.C. Wintersgill, *Ion implantation in polymers*, Nuclear Instruments and Methods in Physics Research Section B: Beam Interactions with Materials and Atoms, 1984, 1(2-3), 595-598
6. P. Ryšánek, P. Čapková, J. Štojdl and col., *Stability of antibacterial modification of nanofibrous PA6/DTAB membrane during air filtration*, Material Science and Engineering, 2019, 96, 807-813
7. M. Mayer, SIMNRA User's guide, Report IPP 9/113, Max-Planck-Institut fur Plasmaphysik, Garching, Germany, 1997.
8. J.F. Ziegler, et al., SRIM: The Stopping and Range of Ions in Matter, Version SRIM2013, Available at: http://www.srim.org/.
9. A. E.Al-Rawajfeh, *Polyamide-based composite membranes: Part 1. Preparation and characterization*, Desalination, 2005, 179(1-3), 265-272
10. Q. Li, Z. Xu, L. Yu, *Effects of mixed solvents and PVDF types on performances of PVDF microporous membranes*, Journal of Applied Polymer Science, 2010, 115(4), 2277-2287
11. J. Gao, J. F. Rusling, D. Zhou, *Carbon-Carbon Bond Formation by Electrochemical Catalysis in Conductive Microemulsion*, The Journal of Organic Chemistry, 1996, 61(17), 5972-5977
12. X. Zhang, M. Renbo, L. Jiang, W. Wei, *Morphology and electrical properties of polypropylene/polyamide 6/glass fibers composites with low carbon black loading*, Journal of Polymer Engineering, 2019, 39(9), 813-821